Results in Engineering 21 (2024) 101670

Contents lists available at ScienceDirect

Results in Engineering

journal homepage: www.sciencedirect.com/journal/results-in-engineering

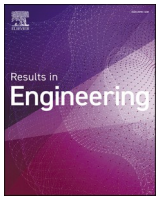

Analysis and simulation of a novel speed estimation method based on oversampling and noise shaping techniques

F. Colodro [a,*], J.L. Mora [a], F. Barrero [a], M.R. Arahal [b], J.M. Martinez-Heredia [a]

[a] Electronic Engineering Department, Universidad de Sevilla, Camino de Los Descubrimientos S/n, 41092, Sevilla, Spain
[b] Systems Engineering and Automation, Universidad de Sevilla, Camino de Los Descubrimientos S/n, 41092, Sevilla, Spain

ARTICLE INFO

Index Terms:
Electrical drives
Frequency modulation
Sigma-delta modulation
Speed measurement

ABSTRACT

Angle measurement is widely used in the servo positioning and speed control of electrical drives, where optical encoders are employed as sensors and coupled to microcontrollers with complex peripherals to provide effective position and speed measurement methods. These methods can achieve high precision and fast response, but are not particularly efficient with computer resources and require high computational costs. Therefore, fast timers, encoder signal oversampling, and a complex post-processing algorithm are used together in a recent research work to achieve a high-precision speed estimation method. Our work will prove that encoder outputs share the oversampling and noise shaping properties typical of sigma-delta modulated signals if they are sampled regularly. Based on this, a new simple and accurate speed estimation method is proposed. Here, encoder outputs are synchronously sampled, differenced, and low-pass filtered. As a result, the speed estimation circuit and its interface with the control unit are greatly simplified, while high accuracy can be achieved. A detailed mathematical analysis of the proposed technique is also performed, and the results obtained are validated by means of a simulation environment using Matlab&Simulink.

1. Introduction

Electric machines have existed since the beginning of the 20th century. Its combination with modern microprocessors and power converters has elevated this technology to an important field of research on drives and generators. Furthermore, new challenges in energy generation and mobility have recently reinforced the development of these technologies [1]. The development trends in the area can be summarized as better designs and controllers to achieve higher power/torque densities in smaller sizes [2]. Motion control and performance monitoring technologies are also key topics in electric drives [3,4], where propulsion and generation applications are considered [5–7].

Sensorless techniques are sometimes used to estimate velocity [8]. However, Quadrature Optical Encoders (QOEs for simplicity), along with microcontroller peripherals, are primarily used for that purpose. Therefore, QOEs can be considered as the basis for position and motion control in electrical systems [9]. Speed estimation using QOEs is based on the counting of encoder pulses and digital state machines with the ability to detect the direction of rotation. A recent review of these methods can be found in Ref. [10], where it is shown that the algorithms used present precision problems due to their asynchronous operation with the speed controller loop. These problems can be mitigated, but require new dedicated hardware, which increases the cost of speed estimation. For example, the hardware responsible for processing the encoder pulses is expanded in Ref. [10]. As a consequence, two capture units of a TMS320F28035 microcontroller are required together with the internal peripheral, the so-called quadrature encoder pulse unit.

The mechanical speed estimate is based on the ratio of the angle increment provided by the encoder, and the time evaluated as the number of ticks of an internal clock; see Eq. (1).

$$w_m = \frac{\Delta\theta}{\Delta t} \approx k\frac{\Delta p}{\Delta c} \tag{1}$$

where k is a constant and p and c are outputs from an encoder pulse counter and a microcontroller timer, respectively, in an internal microprocessor peripheral. Angle and time (integer numbers Δp and Δc) are estimated by means of digital counters. The idea of oversampling for speed estimation is first introduced in Ref. [11], where an oversampled digital differentiator (ODD) is used. There, the encoder pulse counter

* Corresponding author.
E-mail addresses: pcolr@us.es (F. Colodro), jolumo@us.es (J.L. Mora), fbarrero@us.es (F. Barrero), arahal@us.es (M.R. Arahal), jmmh@us.es (J.M. Martinez-Heredia).

https://doi.org/10.1016/j.rineng.2023.101670
Received 16 October 2023; Received in revised form 24 November 2023; Accepted 8 December 2023
Available online 12 December 2023

(signal p) is sampled at a rate N times higher than the desired speed measurement rate f_S (number of estimates per second). Then, an average of this angle is obtained every N samples and, finally, a differentiator is applied to calculate Δp. Similarly, a high-frequency clock is used in Ref. [12] to achieve high resolution in the estimation of Δc. Then, the speed is estimated from Eq. (1) by means of a divider. These estimation methods are based on the well-known constant elapsed time (CET) technique. A variant of the CET method is also used in Refs. [13,14], where the estimation procedure of Δp and Δc dynamically changes as a function of the previous estimates. For this purpose, a clock with a frequency much higher than the required speed measurement rate (f_S) is used to determine time c. Finally, Δc is obtained in Refs. [13,14] using a third-order sinc filter and differentiation, and the speed estimation is obtained using Equation (1).

In general, f_S is not constant and can vary from one estimation to another. In the methods discussed above [11–14], the angle p and the elapsed time c are determined at a frequency rate much larger than the speed measurement rate, f_S. For example, the master clock of the microcontroller (60 MHz) is used to determine c in Refs. [13,14], which implies a large computational burden. On the other hand, it has been suggested in Refs. [13,14], but has not been shown or analyzed, that the generated time sequences have the properties of a sigma-delta modulated signal, which would imply that the errors are spectrally shaped [15]. The Power Spectral Density (PSD) of the speed error, which from now on will be called quantization noise, is zero at DC, increases as frequency does, and takes its maximum value at high frequencies.

In our work, a new speed estimation method is proposed and analyzed using mathematics and simulation. The proposed technique is based on the oversampling of the encoder pulses and on the fact, as will be shown later, that the sequence Δp is a sigma-delta modulated signal if the angle is sampled at a regular rate f_S. Consequently, the proposed method is simple, does not represent a significant computational load, and achieves an acceptable performance. Furthermore, due to regular sampling, the synchronization of the speed estimation and electrical control units are also simplified.

The rest of the work is organized as follows. The proposed speed estimation architecture is presented and analyzed in Section 2, as well as the developed simulation environment and the best performance that can be achieved. In Section 3, the performance achieved for a first-order filtering is calculated and validated by comparing to the simulation results. It is shown that a good trade-off between simplicity (low hardware resources and sampling rate f_S) and performance is achieved for first-order filtering. High-order filters are analyzed in Section 4, where the results obtained prove that performance improves with the order of the filter with a low increase in computational cost. Finally, the conclusions are outlined in Section 5.

2. The proposed speed estimation method

2.1. Architecture of the proposal

The functional block diagram of the proposed algorithm is shown in Fig. 1, where the quadrature square waves outputs provided by the differential encoder $r_X(t)$ ($X = A$ or B) are used as inputs of the peripheral included in modern microcontrollers. Both signals have an instant electrical frequency in Hz proportional to the speed of the rotor, $f_X(t) = N_e\,\omega_m/(2\pi)$, where N_e is the number of pulses per revolution (ppr) and ω_m is the mechanical speed (rad/s). The QOE peripheral generates a sequence of pulses, $r(t)$, at the time of the $r_A(t)$ and $r_B(t)$ edges and includes an asynchronous counter that accumulates a unit every time a pulse occurs, and, consequently, increases at the rate given by Eq. (2):

$$R_c = 4 \cdot f_X = \frac{4 \cdot N_e \cdot \omega_m}{2\pi} \tag{2}$$

The output of the register is sampled at the rate f_S and differentiated to obtain a rough speed estimation. It is shown [16–18] that the differentiator output takes the value given in Eq. (3):

$$\omega_r(n) = \frac{R_c(t)}{f_s} + [q(n) - q(n-1)] = \frac{4 \cdot N_e \cdot \omega_m}{2\pi \cdot f_s} + [q(n) - q(n-1)] \tag{3}$$

where $q(n)$ is the quantization error produced by the difference in pulse width before and after sampling, as illustrated in Fig. 1. It is common to assume that $q(n)$ is a uniformly distributed noise from -0.5 to $+0.5$ whose total power, $P_q = 1/12$, is uniformly distributed in the spectrum from $-f_s/2$ to $+f_s/2$ [15–18]; that is, the power spectral density is given by Eq. (4):

$$S_q\left(e^{\frac{j2\pi f}{f_S}}\right) = \frac{1}{12 \cdot f_s} \tag{4}$$

The rough speed estimation obtained in Eq. (3) can be expressed in the z-domain as in Eq. (5):

$$W_r(z) = \frac{4 \cdot N_e}{2\pi \cdot f_s} \cdot W_m(z) + \left(1 - z^{-1}\right) \cdot Q(z) \tag{5}$$

As expected, the quantization noise is shaped as in a first-order sigma-delta modulation (SDM). Note that the quantization error $Q(z)$ is filtered by the first-order high-pass transfer function $F(z)=(1-z^{-1})$; that is, the error is very small at low frequencies ($F[1] = 0$ in DC) and increases monotonically as the frequency increases, reaching the maximum when the frequency is $f_S/2$ ($F(-1) = 2$) [15].

To remove high-frequency noise, the signal at the differentiator output can be filtered using the low-pass filter $H(z)$ as shown in Fig. 1. The noise power at the filter output can be calculated as in Ref. [15]. Let $G(z)$ be the whole Noise Transfer Function (NTF) that filters the noise, which can be expressed as in Eq. (6):

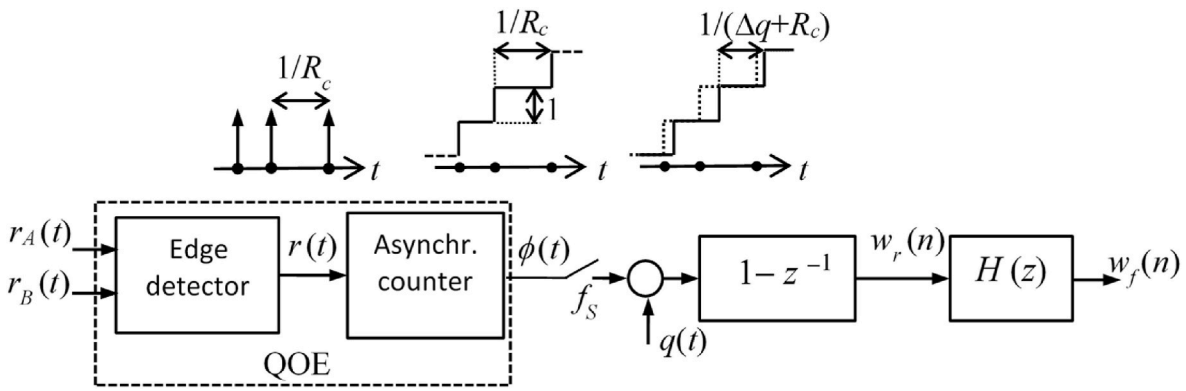

Fig. 1. Functional block diagram of the proposed estimation technique for speed measurement.

$$G(z) = \left(1 - z^{-1}\right) H(z) \tag{6}$$

The noise power can now be calculated by Eq. (7):

$$P_{qf} = \int_{-f_S/2}^{+f_S/2} S_q\left(e^{\frac{j2\pi f}{f_S}}\right)\left|G\left(e^{\frac{j2\pi f}{f_S}}\right)\right|^2 df \tag{7}$$

2.2. Minimum achievable standard deviation

The best performance can be achieved using an ideal low-pass filter. Then, let $H(z)$ be an ideal low-pass filter of bandwidth B and a DC gain given in Eq. (8):

$$g_I = \frac{2\pi f_S}{4N_e} \tag{8}$$

This value has been chosen from Eq. (5) to reach in the filter output a level of signal component equal to the mechanical speed ($\omega_f = \omega_m +$ noise). Due to oversampling, B is much smaller than $f_s/2$ and the approximation given in Eq. (9) can be performed [15]:

$$G\left(e^{\frac{j2\pi f}{f_S}}\right) = \begin{cases} g_I\left(1 - e^{\frac{-j2\pi f}{f_S}}\right) \approx g_I \dfrac{j2\pi f}{f_S} & \text{if} \quad -B < f < +B \\ 0 \qquad \text{otherwise} \end{cases} \tag{9}$$

Replacing Eqs. (8) and (9) in Eq. (7), Eq. (10) can be obtained:

$$P_{qf} = \frac{\pi^4 B^3}{18 f_S N_e^2} \tag{10}$$

Finally, the standard deviation of the noise is given in Eq. (11):

$$STD_{qI} = \sqrt{P_{qf}} = \frac{\pi^2}{\sqrt{18}}\sqrt{\frac{B^3}{N_e^2 f_S}} \tag{11}$$

2.3. Simulation environment

The architecture proposed in Fig. 1 is analyzed using the Simulink environment of Matlab. The model used is shown in Fig. 2, where $r_A(t)$ and $r_B(t)$ are two (out of phase $\pi/2$) square waves of binary values ± 1 synthesized using Voltage Controlled Oscillators (VCOs). To set the instant frequency of f_X, where f_X is given in Eq. (2), both VCOs have a quiescent frequency of $N_e\ W_{off}/(2\pi)$ and a sensitivity (Hz/V) of $N_e\ W_{pk}/(2\pi)$. The product of both signals results in a new square wave of frequency $R_C(t)$. The asynchronous counter is configured to increment one unit on rising or falling edges at the input. The rest of the main path is as in Fig. 1.

An additional signal path has been added (see the upper part of Fig. 2) to evaluate the error of the estimated speed, $e(n)$. The real speed, $w_m(t)$, is time aligned with the coarse estimation, $w_r(t)$, using a delay d-unit, and both are filtered by the same low-pass transfer function. In this way, the error can be calculated by simple subtraction. Finally, the data corresponding to the error and the fine estimation of speed, $w_f(n)$, are saved to a file for post-processing. The Standard Deviation (STD) of the error can be calculated directly in the time domain from $e(n)$ or by spectral analysis of $w_f(n)$ using Matlab. There is hardly any appreciable difference between the results obtained with both methods. PSD is obtained using the Matlab *periodogram* command. The signal and error spectral components (the rest of the components once the signal has been eliminated) can be divided, and from them the signal and noise powers can be calculated.

3. Results and discussions

3.1. Ideal filtering

To validate the theoretical results obtained in Section 2, the proposed architecture has been simulated. The signals $r_A(t)$ and $r_B(t)$ have been chosen for a rotor speed $\omega_m(t)$ with a DC component of $W_{off} = 70$ rad/s, and an AC component of 10 Hz and peak value $W_{pk} = 65$ rad/s. With these values, the rotor speed alternates from low to high speeds (that is, from 5 to 135 rad/s). The rest of the parameters chosen for the simulations are shown in Table 1. The power spectral density of $\omega_r(n)$ is shown in Fig. 3 (upper plot). As can be shown, the spectrum presents two large peaks at the spectral signal components: frequencies 0 and 10 Hz with levels W_{off} and W_{pk}, respectively. Due to oversampling, the error of the estimated speed is spread from 0 to 10 kHz, the latter value being much larger than the signal bandwidth (32 Hz). The noise level is low at low frequencies, but it increases with 20 dB/dec slope as in a first-order SDMs (noise shaping). Therefore, a large amount of this noise can be removed by filtering.

For the given in Table 1, the theoretical STD in Eq. (11) is 0.00119 rad/s and the estimated value from the simulation (Fig. 3) is 0.00122 as long as an ideal low-pass filter is used. Unfortunately, these low values of STD cannot be achieved due to the infeasibility of an ideal filter.

3.2. First-order filter

The transfer function of the first-order low-pass filter is defined as in Eq. (12):

$$H(z) = g_o \frac{1 + z^{-1}}{1 - \alpha z^{-1}} \tag{12}$$

The filter is characterized by α and g_o parameters to fix the cutoff frequency and the DC gain, where the DC gain is chosen to reach a signal component in the filter output equal to the mechanical speed ($\omega_f = \omega_m +$ noise). From Eqs. (5) and (12), Eq. (13) is obtained:

$$\frac{4N_e}{2\pi f_S} H(1) = 1 \quad \rightarrow \quad g_o = \frac{(1-\alpha)\pi f_S}{4N_e} \tag{13}$$

The 3 dB cutoff frequency and α are related by the expressions given in Eq. (14):

$$\begin{aligned} \mathrm{B} &= \frac{\mathrm{f_S}}{\pi}\mathrm{acos}\left(\frac{1+\alpha}{\sqrt{2(1+\alpha^2)}}\right) \\ \alpha &= \frac{1}{2\left[\cos\left(\frac{\pi \mathrm{B}}{\mathrm{f_S}}\right)\right]^2 - 1} - \sqrt{\frac{1}{\left(2\left[\cos\left(\frac{\pi \mathrm{B}}{\mathrm{f_S}}\right)\right]^2 - 1\right)^2} - 1} \end{aligned} \tag{14}$$

In the practical case that $(B/f_S) \ll 1$, the upper equation can be simplified by the approximation in Eq. (15)

$$1 - \alpha \approx 2\pi B/f_S \tag{15}$$

Replacing Eqs. (4), (6), (12) and (13) in Eq. (7) and after making a change of variable $x = 2\pi f/f_S$, the filtered noise power can be expressed as Eq. (16)

$$P_{qf} = \frac{g_o^2}{24\pi}\int_{-\pi}^{+\pi} \left|F\left(e^{jx}\right)\right|^2 dx \tag{16}$$

Where the function F is given in Eq. (17):

$$F(z) = \left(1 - z^{-1}\right)\frac{1 + z^{-1}}{1 - \alpha z^{-1}} \tag{17}$$

It can be shown (see the appendix) that the integral in Eq. (16), as long as $0 < \alpha < 1$, takes the value 4π independently of the actual value of α. So, the noise power and the noise STD are finally given in Eqs. (18) and (19), respectively.

$$P_{qf} = \frac{(1-\alpha)^2 \pi^2 f_S^2}{96 N_e^2} \tag{18}$$

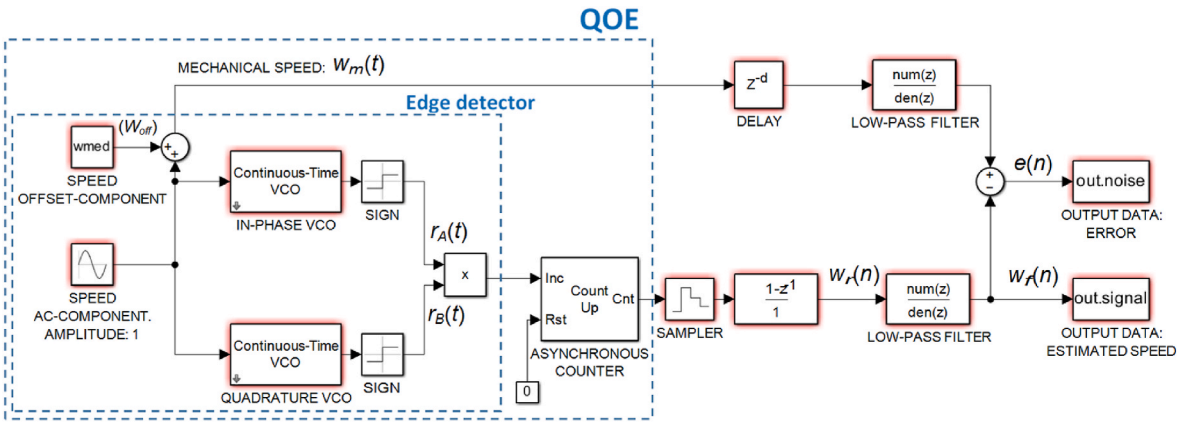

Fig. 2. Simulation environment.

Table 1
Parameters of the system.

B (Hz)	f_S (kHz)	N_e (ppr)	*offset* (rad/s)	*peak* (rad/s)
32	20	2500	70	65

respectively. In conclusion, a resolution of approximately[1] 11.8 effective bits can be achieved with a simple first-order filter, resolution that can rise to 16.6 bits by increasing the filter order.

3.3. Discussion

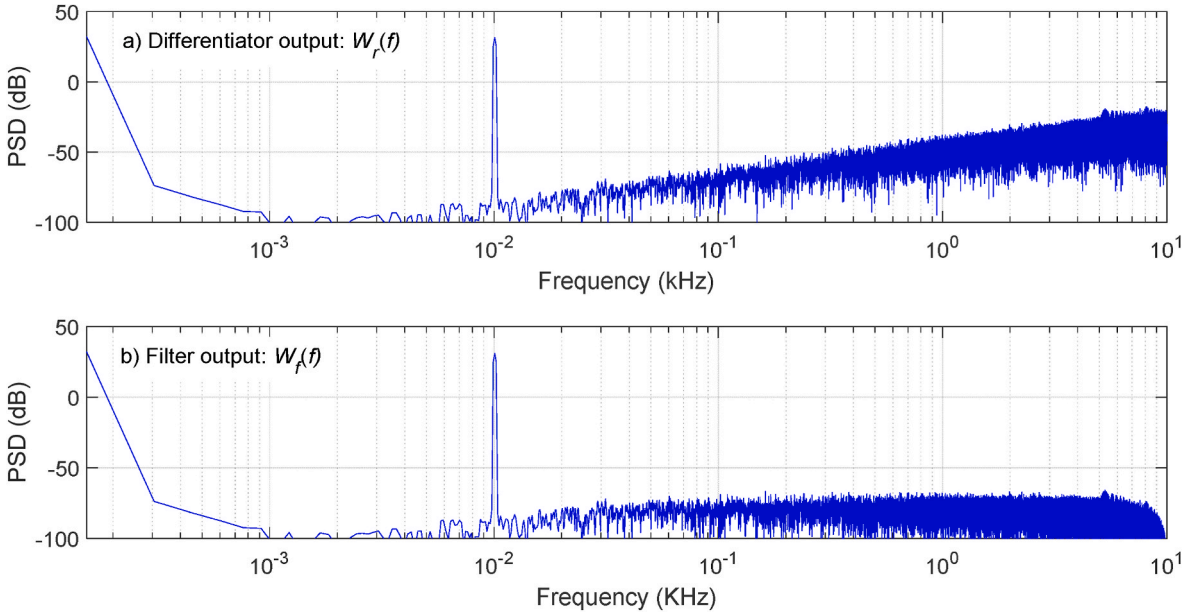

Fig. 3. Power spectral density of signals in the differentiator output (top graph) and in the 1st order filter output (bottom graph).

$$STD_{1st} = \sqrt{P_{qf}} = \frac{(1-\alpha)\pi f_S}{\sqrt{96}N_e} \approx \frac{\pi^2}{\sqrt{24}}\left(\frac{B}{N_e}\right) \tag{19}$$

The approximation on the right side can be derived from Eq. (15). The parameter α has to take the value 0.99 for a cutoff frequency $B = 32$ Hz. The STD calculated from Eq. (19) is 0.0257 rad/s and the value achieved from the simulation is 0.0248 rad/s. Again, the parameters given in Table 1 have been chosen.

The power of the signal component can be obtained by the sum of their DC and AC components, as shown in Eq. (20):

$$P_{wf,S} = W_{off}^2 + \frac{W_{pk}^2}{2} = 7013 \tag{20}$$

The Signal-to-Noise Ratio (SNR), $SNR = 10\log_{10}(P_{wf,S}/STD^2)$, can now be calculated for first-order and ideal filtering, 70.5 and 98.7 dB,

Note that the asynchronous counter in Fig. 1 performs an analog-to-digital conversion, accumulating a unit every time an edge appears in any of the encoder pulses. The larger the N_e, the higher the frequency of the pulse sequence at the counter input and the number of units accumulated for a fixed sampling period, $T_S = 1/f_S$. Therefore, the resolution of this analog-to-digital conversion increases. As expected, the STD noise is inversely proportional to N_e as shown in Eqs. (11) and (19). If the counter content were sampled just at the time instants where the pulses are located at its input, there would be no quantization errors. Thus, the quantization error is due to the sampling instants not being synchronized with the counter edges. The maximum difference between them is T_S. The larger the f_S, the lower the error. But the approximation in Eq.

[1] A 6 dB increase in SNR corresponds to 1 bit more resolution.

(19) does not support this assertion. In the following, this issue is discussed.

It is straightforward to show from Eq. (14) that the parameter α is greater than zero if the condition given in Eq. (21) is hold.

$$cos(\pi B/f_S) > 1/\sqrt{2} \quad \rightarrow \quad f_S > \pi \frac{B}{acos(1/\sqrt{2})} \tag{21}$$

For $B = 32$ Hz, the minimum value of the sampling frequency is $f_S = 128$ Hz. Accurate and approximated expressions in Eq. (19) are represented in Fig. 4 for a f_S interval from 0.2 to 100 kHz (the rest of the parameters are given in Table 1). Note that STD does not even worsen but improves as f_S decreases. The improvement is 3 dB at a frequency of 202 Hz. To verify these results, several simulations have been carried out. The simulation results fit very well with the theoretical ones. For $f_S = 202$ Hz, Fig. 5 shows the waveforms and the spectrum obtained. The differences between the mechanical speed waveforms and the signal at the filter output cannot be appreciated. The noise STD calculated from the simulation is 0.018671 rad/s (−34.5766 dB), value that also fits very well with Fig. 4. In this case, the SNRs calculated from Eqs. (11), (19) and (20) are 73.5 and 78.8 dB for the first-order and ideal filtering, respectively.

If $f_S \gg B$, the STD does not depend on f_S, as shown on the right-hand side of Eq. (19). The signal spectra at the output of the filter and the differentiator are shown in Fig. 3. Both spectra are identical in the filter passband. Outside this band, the filter attenuates noise at a rate of 20 dB/dec, the same rate at which noise increases in Fig. 3 (upper plot). Consequently, the background noise remains flat at a certain level[2] up to the vicinity of the upper frequency; see. Fig. 3 (lower plot). At high frequencies, the zero of $H(z)$ kicks in, canceling the noise at $f_S/2$. Neglecting the contribution to the total power of the noise components around 0 and $f_S/2$, if f_S increases, S_q in Eq. (4) decreases proportionally to $1/f_S$, but the integration interval increases by the same amount; see Eq. (7). Therefore, P_{qf} hardly changes. Only when f_S is not much larger than B, the regions around 0 and $f_S/2$ are a significant portion of the entire spectrum, the contribution to the total power of the region with flat spectrum is smaller, and the STD decreases; see Fig. 5 (lower plot).

4. High-order filtering

First-order filtering has been shown to be a good low-complexity solution for velocity estimation. Since STD is weakly dependent on f_S at high sample rates and, even more, slightly improved at lower sample rates, first-order filtering at low sample rates is recommended. For example, an SNR of 73.5 dB (12.2 effective bits of resolution) can be achieved by lowering the f_S to 202 Hz for the parameters in Table 1. Provided this accuracy is sufficient for the application concerned, a first-class filter order is the simplest solution.

However, compared to ideal filtering, there is Room For Improvement (RFI). Let *RFI* be defined as in Eq. (22):

$$RFI = 20\log_{10}\frac{STD_{1st}}{STD_I} \approx 10\log_{10}\frac{f_S}{B} - 1.96 \tag{22}$$

For the sake of clarity, the approximation in Eq. (19) is used in the second equality. The higher the f_S, the higher the RFI. If f_S increases from 202 Hz to 20 kHz, the *RFI* changes from 6 to 26 dB. Actually, 3 dB must be subtracted from 6 to compensate for the approximation used in Eq. (22) as shown in Fig. 4. The RFI can be improved by high-order filtering. Although, the higher the order, the greater the complexity; many efficient techniques have been developed for high-order digital design [19].

The second order filter is the one immediately higher in complexity than the first order one [20,21]. A Butterworth transfer function with a bandwidth of $B = 32$ Hz has been chosen. In reality, this Butterworth digital filter is implemented in the discrete-time domain [21], but the analysis will be simplified by approximating its amplitude response to that of a Butterworth continuous-time filter [20]. The continuous-time amplitude response is given in Eq. (23):

$$H(f) = \frac{2\pi f_S}{4N_e} \frac{1}{\sqrt{1 + (f/B)^4}} \tag{23}$$

Both responses fit very well up to the vicinity of $f_S/2$, as shown in Fig. 6.

The attenuation is very large at high frequencies (it exceeds 60 dB for frequencies above 1 kHz in Fig. 6). Therefore, the error in the calculation of the integral given in Eq. (7) will be small if the integration interval extends from $-\infty$ to $+\infty$. The STD can now be evaluated from Eq. (7) to obtain the standard deviation achieved with the second-order filter; see Eq. (24).

$$STD_{2nd} = \sqrt{P_{qf}} = \sqrt{\frac{1.11\pi^4 B^3}{6 f_S N_e^2}} \tag{24}$$

In the derivation of Eq. (24) it has been taken into consideration the result given in Eq. (25).

$$\int_{-\infty}^{+\infty} \frac{x^2}{1 + x^4} dx = \frac{\pi}{\sqrt{2}} \approx 2.22 \tag{25}$$

For high sample rates, it can be established from Eqs. (11) and (24) that the STD achieved with second-order filtering is only 1.82 (5.2 dB) times worse than with ideal filtering.

Simulations were run again for $f_S = 202$ Hz and 20 kHz, obtaining an SNR of 75.17 and 92.8 dB, respectively. The improvement, compared to the SNR obtained for the case of the first-order filter, is 1.67 and 21.6 dB, respectively. It is possible to recover up to 21.6 dB over the.

Total RFI of 26 dB for $f_S = 20$ kHz by increasing the filter order by just one unit. Spectra are shown in Fig. 7. Compared to the first-order case, it is difficult to see the differences in Fig. 5 (see lower plot) and Fig. 7 (see upper figure) for $f_S = 202$ Hz. In contrast, the flat noise floor in Fig. 3 (lower picture) is attenuated by an additional 20 dB/dec decay rate for $f_S = 20$ kHz.

Finally, the STDs obtained from the simulation are 0.0142 and 0.002081 rad/s for $f_S = 202$ Hz and 20 kHz, respectively. The corresponding values calculated from Eq. (24) are 0.0216 and 0.002173 rad/s, respectively. For the signal power given in Eq. (20), the SNR is 92 dB, a value very close to the one reached with ideal filtering (98.7 dB).

5. Conclusions

In this paper, a method for speed estimation is proposed and analyzed by means of mathematics and simulations. It is shown how regular sampling of the angle and differentiation make that the resulting signal (ω_r in Fig. 1) has the same properties as signals in a first-order sigma-delta modulator. These properties are oversampling and noise shaping. From this fact, the proposed method can be devised by adding a simple filter as shown in Fig. 1. In general, given the cutoff frequency B, the error STD of the estimated speed decreases with the sampling rate f_S, the encoder pulse's number per revolution N_e and the filter order. Different mathematical expressions, validated by simulation results, have been obtained so that the STD can be related to the above parameters.

The simplest filter that can be used is the first-order one. For the case of study characterized by the parameters given in Table 1, the SNR can achieve up to 73.5 dB (12.3 effective number of bits) for a sampling rate as low as $f_S = 202$ Hz. This SNR is close to the 78.8 dB that can be reached using an ideal filter. In conclusion, first-order filtering is a very

[2] This level is given by 10 $\log_{10}(S_q\ (2g_o)^2)$. At mid frequencies, $(1 + z^{-1})(1-z^{-1})/(1-\alpha z^{-1}) \approx 2$. From Eqs. (4), (13) and (15), the level takes the value 10 $\log_{10}(\pi\ (B/N_e)^2/f_S)$, which is inversely proportional to f_S.

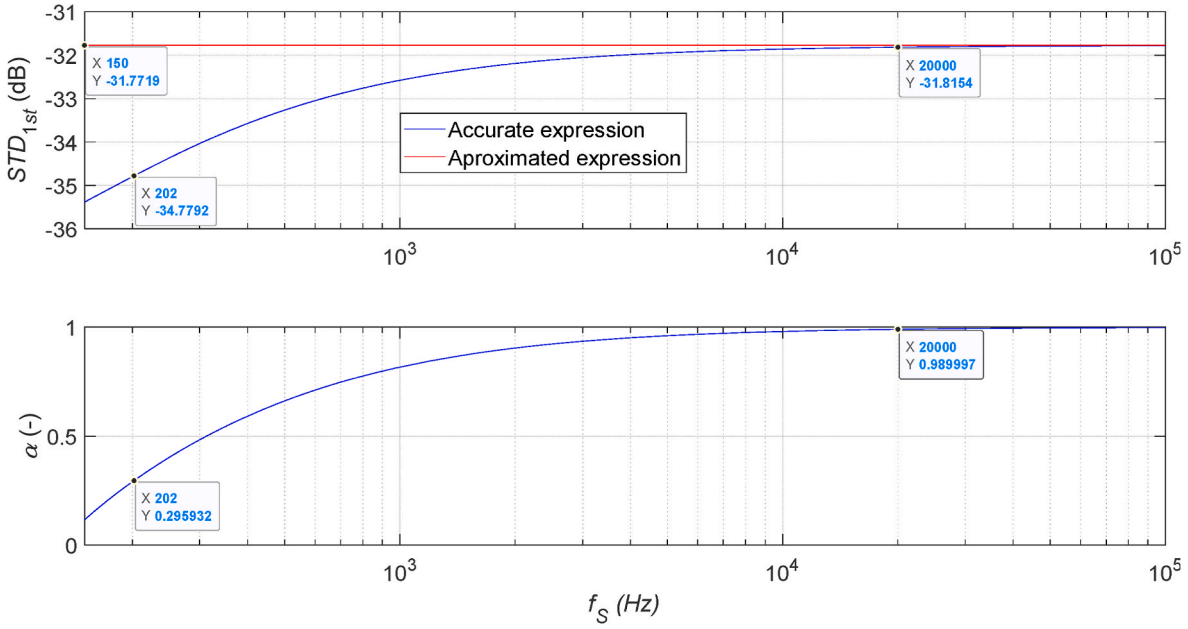

Fig. 4. The upper curves are the standard deviations, 20 $\log_{10}(\mathrm{STD}_{1st})$, given in Eq. (19) and the lower one the corresponding filter parameter, α, versus the sampling frequency.

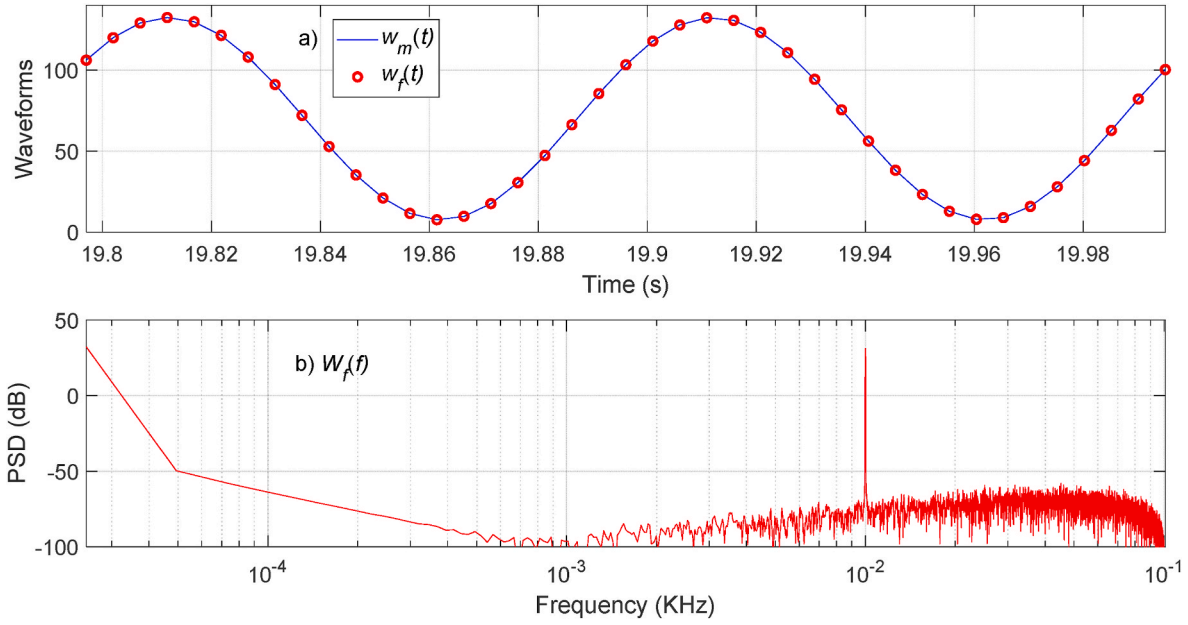

Fig. 5. Using a sampling frequency of 202 Hz, upper plot: waveforms of mechanical speed, $\omega_m(t)$ and signal at filter output, $\omega_f(n)$, lower figure: power spectral density of $\omega_f(n)$.

good choice for moderate resolution, low sampling rate, and low cost in computational resources. If a higher resolution is required, the f_S and the filter order have to be increased. For $f_S = 20$ kHz and a second-order filter, it can be reached at 92 dB (15.3 effective bits). This last value is very close to the one obtained if ideal filtering could be performed (98.7 dB).

One of the main features of the proposed method is its simplicity. The implementation of first- or second-order discrete-time filters at the rates given above does not consume much computational resources in modern microcontrollers. Unlike other published methods, divisions do not have to be performed and the master clock of the system, around several megahertz decades, is not used in the estimation of the speed. Furthermore, the sampling rate can be chosen to be the same as the electrical control-loop timing. Therefore, the estimated speed, ω_r in Fig. 1, is synchronized with the controller, and the integration of the speed estimator and the control block is simplified.

CRediT authorship contribution statement

F. Colodro: Conceptualization, Formal analysis, Methodology, Writing - original draft. **J.L. Mora:** Conceptualization, Software, Validation, Writing - review & editing. **F. Barrero:** Conceptualization, Project administration, Supervision, Writing - original draft. **M.R. Arahal:** Funding acquisition, Supervision, Validation, Writing - review & editing. **J.M. Martinez-Heredia:** Funding acquisition, Software, Validation, Writing - review & editing.

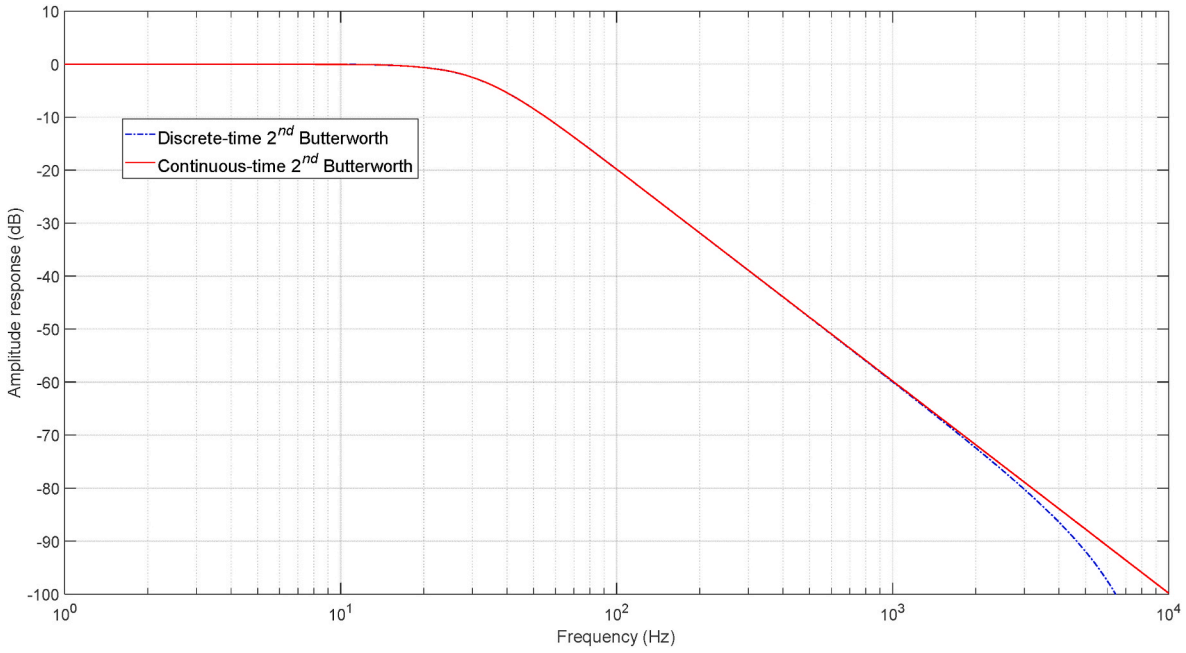

Fig. 6. Amplitude response of a 2nd-order Butterworth filter for continuous and discrete-time cases and for $f_S = 20$ kHz and $B = 32$ Hz.

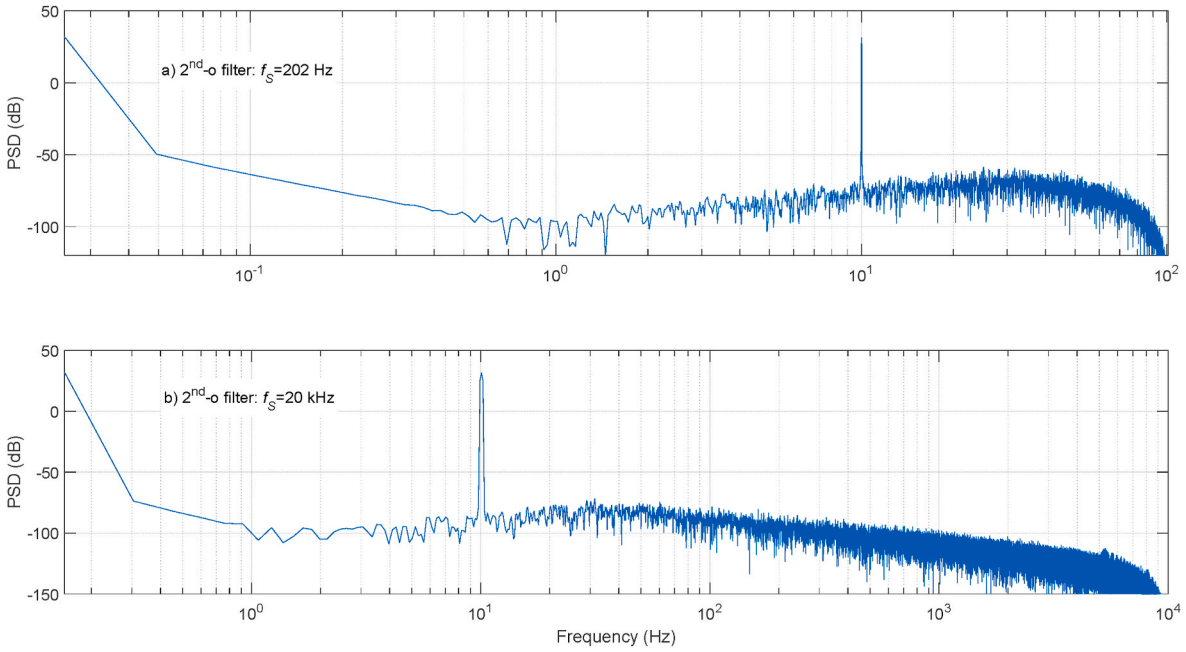

Fig. 7. PSDs at the output of a 2nd-order filter with sampling rates of 200 Hz (top plot) and 20 kHz (bottom picture).

Declaration of competing interest

The authors declare that they have no known competing financial interests or personal relationships that could have appeared to influence the work reported in this paper.

Data availability

No data was used for the research described in the article.

Acknowledgments

This work is part of the Grant TED2021-129558B–C22 funded by MCIN/AEI/10.13039/501100011033 and by the "European Union NextGenerationEU/PRTR". Also, the authors want to thank the support provided by project I + D + i/PID2021-125189OB-I00, funded by MCIN/AEI/10.13039/501100011033/by "ERDF A way of making Europe.'.

Appendix

The integral in Eq. (16), after the variable change $z = e^{jx}$, can be expressed as in Eq. (A.1):

$$\int_{-\pi}^{+\pi} |F(e^{jx})|^2 dx = \oint_C D(z)dz \tag{A.1}$$

where $D(z)$ is given in Eq. (A.2).

$$D(z) = \frac{1}{jz}|F(z)|^2 \tag{A.2}$$

and C is the contour of the unit circle ($|z| = 1$). As long as $F(z)$ is a rational function with real coefficients and is evaluated on C, its complex conjugate is $F^*(z) = F(z^*) = F(1/z)$. So, Eq. (A.2) can be expressed as in Eq. (A.3):

$$D(z) = \frac{1}{jz}F(z)F(1/z) = \frac{1}{j\alpha z^2}\frac{(z^2-1)^2}{z^2 - \frac{1+\alpha^2}{\alpha}z+1} \tag{A.3}$$

$D(z)$ has a double pole in $z = 0$ and, for $0 < \alpha < 1$, one pole more inside C, see Eq. (A.4):

$$z_p = \frac{1+\alpha^2}{2\alpha} - \sqrt{\left(\frac{1+\alpha^2}{2\alpha}\right)^2 - 1} \tag{A.4}$$

The residues of both singularities inside the unit circles are given in Eq. (A.5):

$$\begin{aligned} R(0) &= \frac{d}{dz}\left[z^2 D(z)\right]_{z=0} = \frac{1+\alpha^2}{j\alpha^2} \\ R(z_p) &= \lim_{z\to z_p}(z - z_p)D(z) = \frac{-1+\alpha^2}{j\alpha^2} \end{aligned} \tag{A.5}$$

Finally, the searched result is shown in Eq. (A.6).

$$\int_{-\pi}^{+\pi} |F(e^{jx})|^2 dx = \oint_C D(z)dz = j2\pi\left[R(0) + R(z_p)\right] = 4\pi \tag{A.6}$$

References

[1] R. Qu, Y. Zhou, D. Li, Milestones, hotspots and trends in the development of electric machines, iEnergy 1 (1) (2022) 82–99.

[2] I. Husain, et al., Electric drive technology trends, challenges, and opportunities for future electric vehicles, Proc. IEEE 109 (6) (2021) 1039–1059.

[3] S.B. Lee, et al., Condition monitoring of industrial electric machines: state of the art and future challenges, IEEE Ind. Electron. Magazine 14 (4) (2020) 158–167.

[4] GiM.T. Nguyen, L. Ton-That, Keisuke Fujisaki, Experimental study of mutual effects of high carrier frequency, dead-time and control sample time on IPMSM core loss under SiC inverter excitation, Results Eng. J. 19 (2023), https://doi.org/10.1016/j.rineng.2023.101278.

[5] K. El Mezdi, A. El Magri, I. El Myasse, A. Watil, L. Bahatti, N. Elaadouli, H. Ouabi, Performance improvement through nonlinear control design and power management of a grid-connected wind-battery hybrid energy storage system, Results Eng. J. 19 (2023), https://doi.org/10.1016/j.rineng.2023.101491.

[6] V.B. Murali Krishna, V. Sandeep, S.S. Murthy, Kishore Yadlapati, Experimental investigation on performance comparison of self-excited induction generator and permanent magnet synchronous generator for small scale renewable energy applications, Renew. Energy J 195 (2022), https://doi.org/10.1016/j.renene.2022.06.051.

[7] V.B. Murali Krishna, V. Sandeep, B.K. Narendra, K.R.K.V. Prasad, Experimental study on self-excited induction generator for small-scale isolated rural electricity applications, Results Eng. J. 18 (2023), https://doi.org/10.1016/j.rineng.2023.101182.

[8] X. Chi, C. Wang, Q. Wu, J. Yang, W. Lin, P. Zeng, H. Li, M. Shao, A ripple suppression of sensorless FOC of PMSM electrical drive system based on MRAS, Results Eng. J. 20 (2023), https://doi.org/10.1016/j.rineng.2023.101427.

[9] Y. Vazquez-Gutierrez, D.L. O'Sullivan, R.C. Kavanagh, Evaluation of three optical-encoder-based speed estimation methods for motion control, J. Eng. 2019 (17) (2019) 4069–4073.

[10] A. Anuchin, A. Dianov, F. Briz, Synchronous constant elapsed time speed estimation using incremental encoders, IEEE ASME Trans. Mechatron. 24 (4) (2019) 1893–1901.

[11] R.C. Kavanagh, Signal processing techniques for improved digital tachometry, IEEE Proc. Int. Symp. Ind. Symp. (ISIE) (2002), https://doi.org/10.1109/ISIE.2002.1026342.

[12] R.C. Kavanagh, An enhanced constant sample-time digital tachometer through oversampling, Trans. Inst. Meas. Control 26 (2) (2004) 83–98.

[13] Y. Kazemirova, V. Podzorova, A. Anuchin, M. Lashkevich, D. Aliamkin, Y. Vagapov, Speed estimation applying sinc-filter to a period-based method for incremental position encoder, in: 54th International Universities Power Engineering Conference (UPEC), 2019.

[14] A. Anuchin, V. Podzorova, Y. Kazemirova, H. Chen, M. Lashkevich, D. Savkin, G. Demidova, Speed measurement for incremental position encoder using period-based method with Sinc 3 filtering, IEEE Sensor. J. 23 (5) (2023).

[15] S.R. Norsworthy, R. Schreier, G.C. Temes, Delta-Sigma Data Converters, IEEE Press, New York, 1997, 9781119258278.

[16] M. Hovin, A. Olsen, T.S. Lande, C. Toumazou, Delta-Sigma modulators using frequency-modulated intermediate values, IEEE J. Solid State Circ. 32 (1) (1997) 13–22.

[17] J. Kim, T.K. Jang, Y.G. Yoon, S. Cho, Analysis and design of voltage-controlled oscillator based analog-to-digital converter, IEEE Trans. Circ. Syst. I 57 (1) (2010) 18–30.

[18] F. Colodro, A. Torralba, Frequency-to-Digital conversion based on a sampled Phase-Locked Loop, Microelectron. J. 44 (10) (2013) 880–887.

[19] O. Diouri, A. Gaga, H. Ouanan, S. Senhaji, S. Faquir, M.O. Jamil, Comparison study of hardware architectures performance between FPGA and DSP processors for implementing digital signal processing algorithms: application of FIR digital filter, Results Eng. J. 16 (2022), https://doi.org/10.1016/j.rineng.2022.100639.

[20] Norbert R. Malik, Electronic Circuits: Analysis, Simulation, and Design, Prentice Hall PTR, 2019, 9780023749100.

[21] P.P. Vaidyanathan, Multirate Systems and Filter Banks, Prentice Hall, 1993, 0-13-605718-7.

Francisco Colodro received his Telecommunications Engineering degree from the University of Vigo, Spain, in 1992, and his Ph.D. degree from the University of Seville (US), Spain, in 1997. He is currently a Senior Lecturer in the Department of Electronic Engineering, US. His research interests include analog-to-digital and digital-to-analog conversion, sigma–delta modulators, and microelectronic circuits and systems with application to control, aeronautics and communications.

José Luis Mora-Jiménez received his M.S. and Ph.D. degrees in Industrial Engineering from the US, Spain, in 1992 and 2001, respectively. He is currently an Associate Professor in the Department of Electronic Engineering, US. His current research areas are digital design, modeling and control of power converters, multilevel converters, and sensor-less motor drives.

F. Barrero (researcherID: A-9626-2013, ORCID: 0000-0002-2896-4472) received the MSc and PhD degrees in Electrical and **Electronic** Engineering from the University of Seville, Spain, in 1992 and 1998, respectively. In 1992, He joined the Electronic Engineering Department at the University of Seville, where He is currently Full Professor. He has authored more than 200 research papers and received the Best Paper Awards from the IEEE Transactions on Industrial Electronics for 2009 and from the IET Electric Power Applications for 2010–2011. His research interests include the field of control of multiphase AC drives.

Manuel R. Arahal was born in Dos Hermanas, Seville, Spain 1966. He received the Industrial Engineering master degree in 1991 and the Ph.D. in 1996 both at the Universidad de Sevilla, Spain. He is currently a full professor at the Ingeniería de Sistemas y Automática department in the University of Seville. Prof. Arahal has authored more than 60 published papers in scientific journals and has received the Best Paper Awards from the IEEE Transactions on Industrial Electronics for 2009 and from the IET Electric Power Applications for 2010–2011.

Juana M. Martinez-Heredia received her Telecommunications Engineering and Ph.D. degrees from the University of Seville (US), Spain, in 1999 and 2006, respectively. Since 1999, she has been with the Department of Electronic Engineering, US, where she is an Associate Professor. Her research interests include low-voltage low-power analog circuit design, analog and mixed-signal design, and design of circuits for aircrafts and UAVs